

# The applications of a helical anchor-based thermoelectric generator in a lunar environment

Eliazar Q. Montemayor III\*, Matthew V. Lewton, and Kane C. Timlin

*Department of Engineering, Physical, and Computer Sciences, Montgomery College  
Montgomery County, Maryland, USA*

\*Corresponding author.

Email address: [emontema@montgomerycollege.edu](mailto:emontema@montgomerycollege.edu) (institutional) or [eqmontemayoriii@gmail.com](mailto:eqmontemayoriii@gmail.com) (personal)

---

## ARTICLE INFO

### *Article history* —

Draft completed: 26 March 2021  
NASA Subject Matter Expert  
reviewed: April 2021  
Submitted to arXiv: 26 July 2021

### *Keywords* —

Lunar habitation  
Renewable energy sources  
Soil measurements  
Thermoelectric devices  
Waste heat

## ABSTRACT

With the advent of new technologies and the growing conviction in favor of renewable energy, a marked importance has been placed on utilizing renewable energy sources for long-term use. Coming into play with NASA’s objective to establish a long-term extraterrestrial colony on Earth’s moon as part of its ongoing Artemis program, there is a marked need to utilize advanced technology to sustain the operations of lunar processes. Thermoelectric generators are a form of renewable energy source that converts heat into power. Simulations and experiments were conducted to test the use of a helical anchor-based device relying on such generators. This study aims to determine the feasibility of using thermoelectric technology for the Artemis Base Camp as a way to both dissipate heat away from working processes and to generate power while doing so.

---

## I. INTRODUCTION

The Artemis program is NASA’s next stage in human spaceflight. The program begins with remote and later human-manned lunar expeditions to gather data and test the feasibility of moon life, gradually building up the foundations of a habitable lunar colony and establishing a permanent human presence on the moon, with an overarching plan to set up a gateway station for exploration on Mars [1].

Shackleton, a large impact crater on the lunar south pole, is the prime location for NASA’s Artemis Base Camp [3]. The three main criteria for choosing a site are: that it experiences near-continuous sunlight, that it experiences low-to-moderate temperature swings, and that it provides access to ice-bearing regions. Because of its location, the crater’s rim at the surface is effectively bathed in constant sunlight while its interior is perpetually shadowed; the surface of the lunar south pole has a mean temperature of approximately 250-260 K with more stable recorded values than regions closer to the equator because of the sun’s lengthened presence at the poles. The average temperature of Shackleton’s interior never reaches past 100 K as little heat from the sun enters the crater; these temperatures facilitate the presence of frozen water deep in the crater’s interior.

Lunar soil is characterized as a “silty sand” because of its fine grain size, low density, and elastic behavior; it has a thermal conductivity of approximately 0.003 to 0.009 W/mK [2, 4, 5]. Lunar regolith can be separated into three distinct

regions: the dust and soil layers — collectively referred to as the upper lunar regolith — and the bedrock layer. The dust layer is a thin blanket of sand-like grains spread across the surface up to a depth of 2 cm, atop the soil layer that reaches to between 5 and 10 meters down. The upper lunar regolith is characterised by a high void ratio and porosity with an increasing bulk density from around 1.3 g/cm<sup>3</sup> at the surface to a high of approximately 2.1 g/cm<sup>3</sup> [4].

Due to the moon’s thin atmosphere and the thermally insulative behavior of the first 20 cm of lunar soil, there exist substantial temperature differentials between the lunar surface and subsurface [2]. NASA field tests done on the Apollo 15 and 17 missions demonstrated the existence of a thermal difference between the lunar surface and subsurface. According to the Lunar Sourcebook, the Apollo 15 and 17 drilling experiments found that temperatures 35 cm and lower beneath the lunar surface stabilize and are not subject to the monthly temperature fluctuations found at the moon’s surface [2]; prior research and analysis suggests that the thermal difference at the equator between the surface and subsurface could be up to 150 K, stabilizing at depths beneath 20 cm [4].

Many different possible power sources are being investigated for their suitability for the Artemis Base Camp. The use of solar energy has been proposed for use in the Base Camp because of its renewability, reliability, and sustainability. Currently, NASA is working with the US Departments of Energy and Defense to establish a power plant

## Nomenclature

### Symbols

$\rho$	Bulk density (g/cm <sup>3</sup> )
$Q$	Heat energy (J)
$\phi_q$	Heat flux (W/m <sup>2</sup> )
$k_c$	Phonon conductivity (W/mK)
$P$	Pressure (psi)
$S$	Seebeck coefficient (V/ K)
$\Delta T$	Temperature gradient/differential (K or ° C)
$k$	Thermal conductivity (W/mK)
$\Delta V$	Voltage drop (V)

### Abbreviations

HTB	Heat transfer block
OCV	Open-current voltage
TEG	Thermoelectric generator
LSII	<i>Lunar Surface Innovation Initiative</i>
MMRTG	<i>Multi-Mission Radioisotope Thermoelectric Generator</i>

to provide power for immediate use and long-term storage through nuclear fission [8].

Another proposed source of power comes through heat. Utilizing the principles of the thermoelectric effect, the thermoelectric generator (TEG) takes advantage of an applied temperature gradient to generate electrical current [9]. Modern TEGs are made of semiconductor material as opposed to traditional metal conductors due to metals' tendency to have increasing electrical resistance with increasing temperatures — and semiconductors' tendency to achieve the opposite effect, as well as semiconductors' generally higher Seebeck coefficients. While the use of metal for TEG technology would adversely facilitate Joule heating and thus a loss in efficiency, the use of an appropriate semiconductor material can lead to an increasing efficiency with an increasing temperature and notably an increasing temperature gradient between the thermoelectric module's two sides [10].

A generalized analysis of the three potential energy sources for the Artemis program demonstrate that — in terms of efficiency — nuclear power takes the lead (ranging on average at 33-37% with a maximum of 94%), followed by solar power (on average 15-20% with an upper limit of 33%), and then thermoelectric power (typically 5-8%, with an expected increase over the years due to emerging technologies) [11, 12, 13, 14]. Unlike nuclear and solar power, TEGs do not have a set upper limit for efficiency; a major parameter in a TEG's maximum efficiency comes from the temperature gradient applied across it [10].

Despite their typically lower system efficiencies, the benefits of TEGs include their maintenance-free and solid-state operation, compact size, and their use in direct energy conversion from heat to electricity [11].

This paper aims to investigate the feasibility of TEG use for long-term power generation in a lunar environment, especially in consideration to its application to the Artemis Base Camp. While numerous studies have already detailed the workings, structure, optimization, and design of TEGs, this paper aims to put into practice this form of energy source with

specific application to long-term power generation as part of the Artemis Base Camp. This paper is organized as follows: Section II describes the authors' intent and purpose in pursuing this avenue in research, Section III explains the design and setup of the produced testing rig for simulation and experimentation, Section IV reports on the results of the simulations and experiments, and Section V closes the paper with a discussion of the conclusions drawn from data analysis, expected feasibility of the design in use, and recommendations for future work.

## II. AIM AND METHOD

Over time, as the Artemis program unfolds and key steps for the program's development are met, NASA's lunar base will be expanded to develop more and more machinery and equipment that allow it to undertake a greater variety of tasks, with gradually decreasing reliance on support from Earth. According to NASA's Plan for Sustained Lunar Exploration and Development [3]:

In addition to testing our systems for the first mission to Mars, a core purpose of Artemis Base Camp will be to demonstrate new technologies that, over time, will expand our capabilities and reduce the costs of lunar operations. Astronauts at Artemis Base Camp will be testing a wide set of new technologies in six priority areas encompassed by the recently announced Lunar Surface Innovation Initiative [such as] surface power; extreme access; excavation and construction; lunar dust mitigation; and extreme environments... For example, ISRU will enable the production of fuel, water, and/or oxygen from local materials, enabling sustainable surface operations with decreasing supply needs from Earth.

Such an increasingly complex system of operations would require continuous power to support it and would also emit high amounts of heat into the environment. This research project relies on the application of a TEG to power future self-sustaining lunar colonies with renewable energy, with a plan to be implemented in the later stages of the Artemis program.

Presently, TEGs are utilized extraterrestrially in mobile units such as rovers and space probes via the specialized Multi-Mission Radioisotope Thermoelectric Generator (MMRTG) designed as a small attached module; the MMRTG generates electricity by capturing radiation from decaying plutonium [15].

We develop a top-down system of power generation with an aim to embed this process into other operations within the Artemis Base Camp, using the waste heat emitted by those other processes as the heat source for our TEGs. By establishing the heat sink below, where the cold side of the TEG is either directly or indirectly in contact with lunar soil, we can rely on the natural conduction of the soil with its —

for our purposes — essentially limitless heat capacity to maintain the temperature gradient; this allows for the dual purpose of recycling otherwise-wasted heat back into the operating cycle of in-situ equipment as well as provide a natural passive heat exchanger by which heat can be dissipated into the environment, away from the Base Camp and its devices.

The capability of this proposed TEG to utilize short-distance temperature gradients allows it to be used in virtually any lunar setting. Taking account of various operations that are planned to be added to the Base Camp to sustain it, its occupants, and NASA’s research missions long-term — as outlined by the Lunar Surface Innovation Initiative — this project will serve the dual purpose of diverting built-up heat from the use of such operations into the surrounding lunar soil and generating more power for the Camp [7].

Our goal is to utilize breakthroughs in thermoelectric technologies and apply that knowledge to develop a working TEG model that can efficiently convert heat into electricity to passively generate power without the need for continuous maintenance, while also providing an opportunity for that intake of heat to be ejected into the surrounding environment to dispel it from the Base Camp.

To this end, we investigate the results of our model by using a combined system of CAD analysis and experimental testing. By utilizing both simulated programs and actual experimentation, we can both develop a working basis of our design’s thermodynamic capabilities in an idealized situation and take into account the flaws of and discrepancies within in-situ operations.

### III. DESIGN

#### A. Thermal Properties of Lunar Soil

The relationship between lunar soil thermal conductivity and temperature for both the dust and soil layers on the moon can be modelled by the equation:

$$k = k_c * (1 + \chi * (T / 350)^3) \quad (1)$$

where  $\chi = 1.48$  in the dust layer and  $\chi = 0.073$  in the soil layer and  $T =$  subsurface temperature in K [4].

It has also been found that thermal conductivity increases with increasing bulk density [4]. The average bulk density of lunar soil increases with increasing soil depth. Where  $z =$  soil depth in cm, this relationship is modelled by the equation:

$$\rho = 1.92 * (z + 12.2) / (z + 18) \quad (2)$$

The general thermal conductivity equation describes the relationship between thermal conductivity, contact surface area, and thermal gradient by the equation:

$$k = Qd / (A * \Delta T) \quad (3)$$

where  $Q$  is the amount of heat transferred across two contacting materials,  $d$  is the thickness of each material,  $A$  is the contact surface area between the two materials, and  $\Delta T$  is the thermal gradient across the two. In a thermally-stabilized system,  $Q$  is a constant value in the entire system.

Equation (3) demonstrates an inverse relationship between thermal conductivity and temperature gradient; this means that a material with a higher thermal conductivity will result in a smaller thermal gradient across its two ends when heat is transferred across it.

By fragmenting the lunar regolith into discrete horizontal layers with constant, infinitesimal thickness  $dz$  from the surface and downward, it can be noted that each instantaneous increase in soil depth leads to an increasing bulk density uniform within each successive layer, as described by Equation (2), and transitively an increasing thermal conductivity; as  $k$  in each successive layer of soil increases,  $\Delta T$  must decrease in turn.

Since  $Q$  is applied from above the surface and transfers downward, it must be true that the very surface of lunar regolith must have a relatively higher thermal gradient across it, where the temperature on top is higher than the temperature below. This lower temperature then becomes the “higher temperature” for the next successive layer — as each layer of soil is applied with an increasing bulk density and an increasing thermal conductivity, the thermal gradient must gradually decrease, resulting in the observed sharp decline in temperature from the surface to about 2 cm in depth, levelling off to a stabilized temperature.

Thus, a natural thermal gradient exists within the lunar subsurface. At the equator, using data collected at the lunar mid-day, temperatures at surface level rest at a mean of 390 K; these values gradually level off to 240 K from depths of 20 cm and onward [4]. Surface temperatures at the equator are more extreme and dependent on the sun’s influence, reaching a high of past 400 K and dropping to a low of 100 K, but this extreme change is only present at the dust layer — at increasing depths in the soil layer, the temperature is maintained with the described 240 K. While temperatures at the lunar south pole may not maintain the same values, a similar relationship between the surface and subsurface there is expected to persist.

#### B. General Design

The thermoelectric module is housed in a helical anchor, a hollow metal cylinder that acts as the framework for the model. Helical anchors are a proposed method of structural support for lunar civil structures due to their

reliability in use as structural supports while maintaining ease of installation as they are installed with screw-in methods using rotary equipment, eliminating the need for large-scale excavation [5].

The thermoelectric module rests on a copper heat transfer block (HTB), a very high thermally-conductive metal, which will facilitate heat transfer between the thermoelectric module and the equally thermally-conductive radiator cylinders below it. The radiator cylinders are thin sheets of thermally-conductive metal that act as standard radiator fins which revolve around the center axis of the system and sit in a concentric fashion to allow for installation into the ground during assembly. The radiator cylinders will be pressed against the HTB within the helical anchor to absorb heat and transfer it to lunar soil filling the gaps between the cylinders.

The helical anchor is insulated along its inner radius at depths above 50 cm to prevent heat in-flow from the sides. The TEG module, the HTB, nor any other component supported within the helical anchor would actually come into contact with the anchor's metal itself, instead pressing against the insulation; this layer of insulation is meant to prevent heat bleed between the inside of the anchor and the outside of the anchor mid-way into the system, allowing for a strict top-down transfer of heat. The heat sink's radiator cylinders and HTB maintain minimum ground temperatures at any depth, even at or above surface level. In actual use, the HTB can be extended above surface level if necessary to reach an external heat source.

To facilitate installation without the necessity of excavating soil, a screw-in system is meant to be utilized with high-torque rotary equipment, much like the installation technique used for deep-foundation helical anchors.

### C. Experimental Design

To model the TEG helical anchor design experimentally with available materials and resources, a proof of concept model was built to test whether the proposed system can effectively produce a temperature differential and electric power in a simulated lunar environment. It is structured in four distinct metal parts: a steel pipe for the anchor, two concentric copper "radiator cylinders" that sit inside the anchor, and a copper block for the HTB.

The helical anchor is modelled with a steel pipe of roughly the same material, diameter, length, and wall thickness, as steel pipes are more readily available than helical anchors. The corresponding helical plates are omitted as those do not significantly affect thermodynamic performance of the radiator cylinders. The helical anchor dimensions were sourced from Led Klosky's Behavior of Composite Granular Materials and Vibratory Helical Applications which provides a recommendation of size specifications for helical anchors in use as deep-foundation support on lunar regolith [5]; however, these dimensions can be modified in any way necessary in practice.

The steel pipe is 72 cm long and extends to a depth of 65 cm, but approximates the thermal performance of any length helical anchor.

The two concentric copper cylinders are 60 cm long and extend to the same depth as the steel pipe. The top of the copper HTB sits at the surface, but could theoretically be at any height with minimal effect on heat flux due to copper's high thermal conductivity.

The TEG module consists of four square TEGs which sit on top of the HTB. The remaining exposed surface of the HTB is covered with ceramic fiber insulation. The ceramic fiber extends along the inside of the steel pipe to a depth of 30 cm.

The TEG module could be optimized by making the top of the HTB a three-dimensional shape, where TEGs can be lined along its surface. However, that only applies if the specific heat source can transfer thermal energy isothermally.

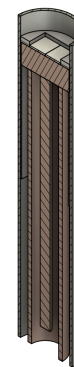


Fig. 1. Cross-sectional image of the experimental model.

### D. Testing Apparatus

In the experiment, the lunar environment is simulated by an acrylic box at a near-vacuum state, which forms the basis for the experimental testing rig. The TEG model is rested isometrically between the four walls and bottom of the box by one pipe diameter from each side. The lunar soil is simulated with dry sand which mimics lunar regolith's small grain size, abrasiveness, and thermal conductivity.

To simulate the effectively infinite heat capacity of lunar soil, an external liquid cooling system is embedded in the subsurface layer of the testing rig. The coolant flows through copper pipes coiled around the walls of the acrylic box below the 20 cm depth where the lunar soil's temperature stabilizes. The cooling system maintains room temperature of the coolant, removing however much heat is applied to the system by the heat source.

In addition, an external portable vacuum pump is used to create a near-vacuum inside the acrylic box to eliminate convective heat transfer at and above the surface.

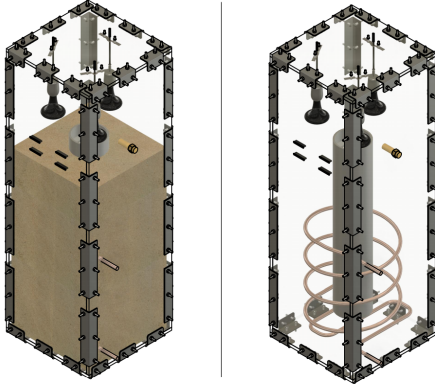


Fig. 2. CAD model of experimental testing rig with and without sand.

Electronic components other than the TEG units are not included in Fig. 2. Slits and holes are in the acrylic box to allow external components to be connected to the testing rig.

For the purposes of experimentation, the source of heat is simulated by heat lamps situated above the soil's surface, emitting heat directed at the soil surface. The outer walls of the acrylic box are insulated with ceramic fiber to eliminate convection cooling or heating of the acrylic box and the heating/cooling systems by external factors.

The testing rig is built both in a true experimental capacity with materials sourced from various manufacturers and digitally within a Fusion 360 CAD model. The system modelled with the CAD program is meant to provide an approximation of and validate the temperature differential to be found in the true testing rig. While Fusion 360 cannot account for the heat removed by the Seebeck effect as electricity, it does provide an indication of how much heat would transfer across the model otherwise.

Nominal thermal conductivity values for each component for the testing rig are provided in the table below:

**Table 1**  
Approximated nominal thermal conductivity values in the experimental testing rig.

Name	Thermal conductivity (nominal, W/mK)
Thermoelectric generator (TEG)	1.5
Dry sand	.25
Copper	400
Stainless Steel (AISI 304)	16
Ceramic Fiber	0.20
Acrylic	0.19

An image of the completed build showing the testing rig and the external cooling system is provided in Fig. 3.



Fig. 3. Image of the completed testing rig with ceramic fiber insulation of one wall stripped away to show components within the testing rig.

#### E. Data Collection

Electronic temperature sensors are slotted through slits in the walls of the testing rig and are embedded equidistant from one another along a vertical plane extending radially from the central axis of the testing rig. Since the system is structured isometrically referencing from the TEG model at the center of the rig, every vertical plane extending radially from the center is essentially a rotated duplicate of one another. The temperature sensors record the temperatures of the various components within the system, feeding them into an Arduino outside the rig. These values provide an indication of temperatures at different locations, the resulting thermal gradient across the system, as well as an overview of the direction of heat flux.

The data collection system is composed of a Raspberry Pi and an Arduino UNO. The temperature sensors plug directly into the Arduino which connects to the Pi through USB. The Pi can divide up the constant stream of characters from the Arduino through certain predetermined signal characters in between each temperature measurement. The measurements from the temperature sensors are then written into a CSV file on the Pi's hard drive.

To measure voltage and power output, a circuit runs the power from the TEG modules through a set amount of resistance with resistors, which are reported in Table 3 of Section IV. Then, the voltage across the resistors is measured, from which the current and power produced by the TEG modules can be determined.

An open-source library designed to work with our specific model temperature sensor is used to read the temperature from the temperature sensors.

## IV. RESULTS

### A. Simulation Results

Prior to conducting in-situ experimentation, the testing rig was modelled and simulated in Fusion 360. This provides a generalized idea of the expected thermal gradient that develops in the actual experiment.

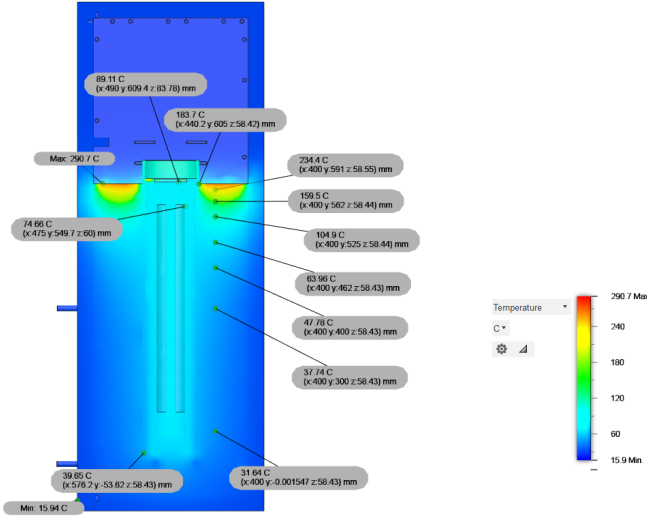


Fig. 4. Simulation result with 750 W.

The parameters of the simulation, to model the conditions of the actual experiment, are as follows: all power from the heat lamps is applied evenly across the sand surface and exposed portions of the TEG anchor, all heat from the heat lamps is absorbed by exposed surfaces via radiation with emissivities appropriate for the materials, all materials start at a room temperature of 20° C, the cooling system maintains 20° C and may remove up to 1500 W of heat from the system, and the ceramic fiber is cooled by convection with the ambient air at 20° C.

Seven simulations are done with increasing heat power put into the system in increments of 150 W (including a simulation of 500 W).

The temperature differential across the TEG is defined as the absolute difference in resulting temperature between the top surface/hot plate (recorded in Fig. 4 as 89.11° C) and the bottom surface/cold plate (74.66° C in Fig. 4) of the TEG module. The temperature differential across the system is defined as the absolute difference in resulting temperature between the top surface of the TEG and the bottom end of the steel anchor (31.64° C in Fig. 4). The results of all seven simulations are noted in Table 2. Sensor readings correspond with sensor locations in Fig. 5.

Table 2

Simulated temperature differential (in ° C) across the device.

Sim No.	Input heat power (W)	Temp. of top TEG surface	Temperature differential across the TEG	Temperature differential across the system
1	150 W	38.81	2.89	16.35
2	300 W	53.52	5.79	29.27
3	450 W	66.14	8.70	40.43
4	500 W	70.03	9.66	43.89
5	600 W	77.45	11.60	50.50
6	750 W	89.11	14.45	57.47
7	900 W	97.57	17.37	68.53

Results from the simulations confirm predictions for soil. Temperatures reach their maximum values at the surface of the simulated sand, which decline sharply even before reaching 20 cm in depth — a similar drop-off to what is expected for true lunar soil. As expected, the thermal gradient of the system stabilizes in a top-down manner; the highest values are observed at the top of the system, with numbers gradually decreasing as depth increases to its maximum value at the bottom. The lowest temperatures can be observed against the walls and at the lowest point of the system; these observations come from scaled heat dissipation of the installed cooling system and support the predicted direction of heat flux in a true lunar system.

The increase in input heat power in each successive simulation seems to affect the resulting temperatures by a significant quantity. The data indicates a linear increase in some notable values; as the input heat power increases, the corresponding TEG top-surface temperature and thermal gradients experience a linear increase as well. The linear increase in temperature differential across both the TEG and the system as a whole indicates that the temperature of the top surface of the TEG grows at a faster rate than both the bottom TEG surface, and the bottom end of the device as a whole.

The simulations did reveal inefficiency caused by the TEG module's square shape. The inconsistent width of the ceramic fiber with respect to the central axis of the system and the inner radius of the steel leads to uneven heating of the TEGs. This demonstrates that the optimal TEG geometry for this system is circular in shape and centered around the central axis, with a ring of ceramic fiber around its edges to insulate it from the steel anchor.

Another major issue that seems to arise is the steel anchor itself: the ceramic fiber blanket lining the anchor's inner radius is too thin to allow for strong enough insulation that heat does not transfer between the inside and outside of the anchor at its upper end. A thicker and less thermally conductive insulative blanket, as well as a less thermally

conductive metal anchor material, would lead to a lower temperature value for the underside surface of the TEG, increasing the resulting temperature gradient. Because of the insulation's lower-than-expected effect, the steel anchor seems to heat up the soil both inside and outside it, indicating the need for greater insulation to prevent heat bleed.

**B. Experimental Results**

Corresponding with the performed simulations, the design was also tested experimentally. Utilizing funding from both NASA and Montgomery College, the testing rig described in Section III is built and assembled with parts obtained from a variety of manufacturers. 10 electric temperature sensors are placed in various contact points shown in Fig. 5. The location of the contact points correspond with temperature probes in the simulation as shown in Fig. 4. The results of two experiments are presented in this paper. While a third trial, prior to the presented two, was conducted, it was unfinished due to issues encountered during testing and its incomplete data was discarded.

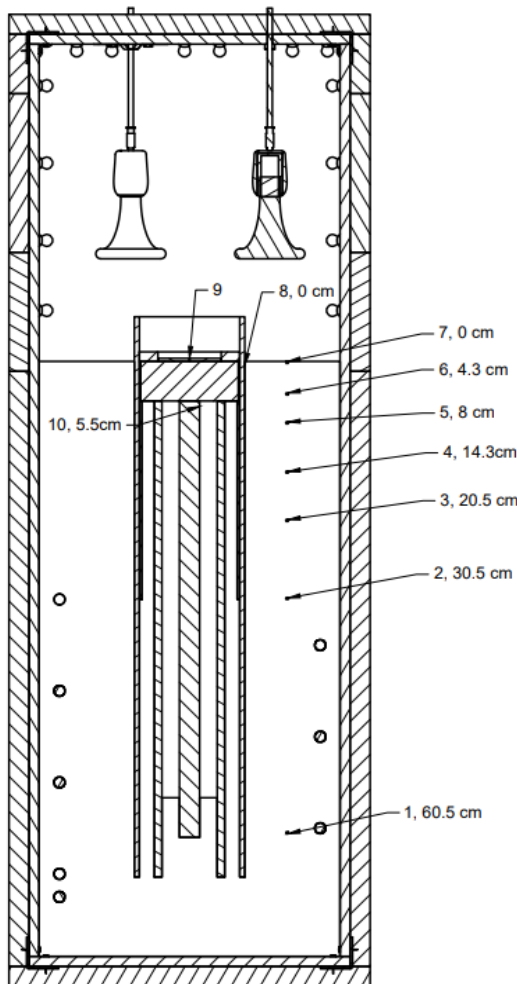


**Fig. 5.** Contact points for the 10 experimental temperature sensors and corresponding depths.

The in-situ testing rig differs in minute details from the on-paper design because of issues encountered during the design process. Although the simulations ran under the assumption of a perfect vacuum state, the inner pressure of the testing rig during testing while the vacuum pump was applied stabilized at about 1-3 psi, down from a natural atmospheric pressure of about 14.7 psi. The four TEGs are connected in series, so the total voltage supplied should be four times as much as what is produced by a single TEG with the same temperature differential.

From the starting time up to a certain point in each time interval, recorded temperatures varied as the input heat caused the formation of a top-down temperature gradient across the system. Time = 0 is defined as the starting time of each experiment, set at when the heat lamps are turned on. Table 3 presents the data of the constant conditions present before and during each experiment; all of the sensor values recorded roughly ambient temperature before the start of each experiment.

**Table 3**  
Constant conditions before the run of each experiment.

Exp No.	Input heat power (W)	Ambient room temperature (° C)	Circuit resistance (kΩ)
1	750 W	20.1	9.4
2	500 W	21.7	9.4

Table 4 presents the averaged temperature values recorded by the temperature sensors during each experiment after the time of stabilization.

**Table 4**  
Stabilized temperature values recorded per sensor for each experiment.

Exp No.	Temp. (° C) at Sensor No.									
	No. 1	No. 2	No. 3	No. 4	No. 5	No. 6	No. 7	No. 8	No. 9	No. 10
1	24	19	21	30	22	35	108	41	83	71
2	27	21	24	29	25	31	104	33	56	43

Time-incremented temperatures for each sensor, for Exp No. 1 and No. 2, are also graphed in Fig. 6 and Fig. 7. The final temperatures recorded in Figs. 6 and 7 correspond with the values presented in Table 4.

Sudden troughs in the temperature data at specific time intervals can be noted in the graph of Fig. 6: these indicate the time intervals when the near-vacuum state of the testing rig would break and air would flow into the vacuum chamber. The gradual rise in temperature after such breaks

indicates the pressure returning to a near-vacuum state as the opening is sealed and the chamber is isolated.

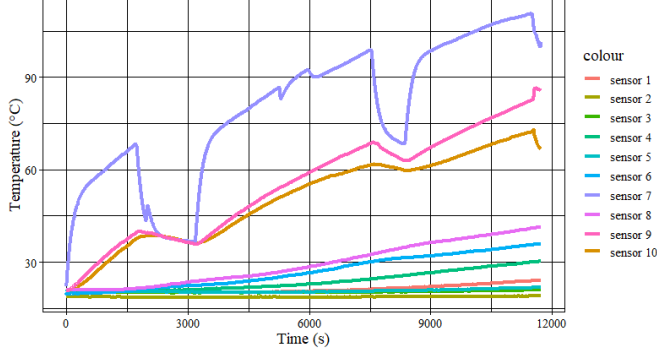


Fig. 6. Time-incremented temperature readings from sensors for Exp No. 1, with a heat input of 750 W.

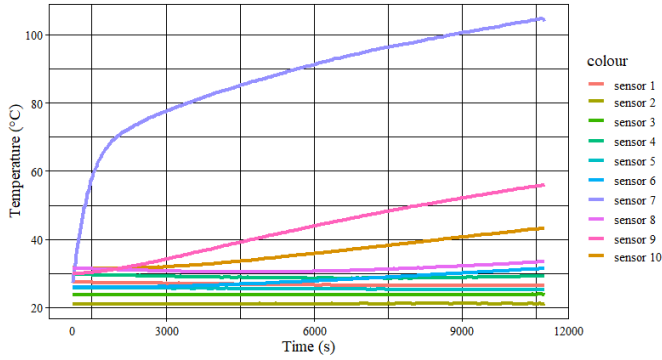


Fig. 7. Time-incremented temperature readings from sensors for Exp No. 2, with a heat input of 500 W.

As with temperature readings, recorded voltage and power were measured during the experiments as well. Time-incremented graphs of voltage and power for Exp No. 1 and No. 2 can be found in Figs. 8 and 9. The voltage and power readings indicate the voltage drop and power dissipation across the resistors of the circuit, as mentioned in Section III, Subsection E. Stabilized readings should be treated as the final recorded values in the following graphs.

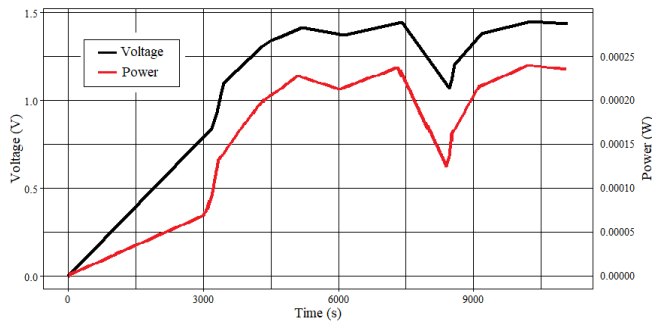


Fig. 8. Time-incremented voltage and power readings for Exp No. 1.

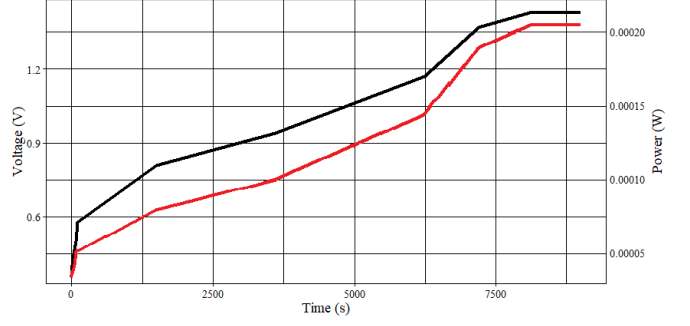


Fig. 9. Time-incremented voltage and power readings for Exp No. 2.

The graphs from Figs. 6 to 9 suggest that the general trends for temperature (of sensor 7), voltage, and power correspond to one another. While voltage and power actually correspond to the temperature *differential* present across the TEGs, these graphs demonstrate the efficiency of the radiator cylinders as the temperatures of the TEG hot plate are allowed to rise while the temperatures of the TEG cold plate are kept to low temperatures — again demonstrating that, as noted in Subsection A of this Section, the temperatures of the TEG’s surface increase at a higher rate than temperatures below it. These graphs also validate the relationship between voltage and temperature gradient from the TEGs through the Seebeck effect as described by the equation:

$$V_{out} = -S * \Delta T * n \quad (4)$$

where  $S$  is the net Seebeck coefficient in both the P-type and N-type semiconductor of each thermocouple in a TEG, and  $n$  is the number of thermocouples connected in series in a TEG [17].

The power delivered to a load in a TEG-based circuit is described by the equation:

$$W = (V_{out})^2 * R_L / (R_{TEG} + R_L)^2 \quad (5)$$

where  $V_{out}$  is the total output voltage supplied by the TEGs,  $R_L$  is the electrical resistance of the load — in our case, the resistors — and  $R_{TEG}$  is the internal electrical resistance of the TEGs [17]. There were no available specifications for the internal resistance of the TEGs, so an internal resistance of 0 Ohms was assumed.

A reason why the voltage was less than expected was because every so often, the box would develop a slight air leak due to problems with the vacuum chamber design. Such leaks would let room temperature air into the chamber, causing the temperature at the surface to dramatically reduce. This accounts for the sudden drops in temperature on the surface-based sensors and also explains why the subsurface sensors were not affected.

### C. Simulation vs. Experiment Discussion

While the simulations predicted higher overall temperatures than were actually recorded in the experiment, the temperature differentials across the TEG were very close to the predicted values. This error is likely because the simulations did not account for radiative heat loss in the vacuum before the heat reached the sand. Additionally, the sand in the simulations has a constant thermal conductivity whereas realistically, the sand's conductivity increases with depth due to an increase in bulk density, comparable to the changes in conductivity for lunar soil as described in Section III, Subsection A. These factors would cause lower overall temperatures in the experiments as well as temperature stabilization at higher depths than in the simulations, as the data supports. Additionally, the simulations assumed that heat was distributed evenly across the sand and TEG surface; however, it is likely that heat pockets formed in the sand during the experiments.

The difference between expected and recorded temperatures is the most drastic near the surface, and decreases with depth. The experimental temperatures that were recorded stabilized below a depth of 20 cm at sensor 3, modeling the actual lunar soil's stabilization at 20 cm while the simulated temperatures did not.

The experimental model's more effective temperature stabilization explains why its temperature differential is the same as the simulation while having much lower overall temperatures at the same wattages. In a cooler, more stabilized environment below 20 cm, the radiator cylinders were more effective at dissipating heat and cooling the HTB in the experiment than the simulation modeled.

Further simulations with theoretical optimized variants of the design, not reported in this paper, found that the main limiting factor for the resulting thermal gradient was the thermal conductivity of the TEG. The area of contact with the TEG is where the HTB is most vulnerable to heat flow as that area warms the entire radiator cylinder system. The TEG units used had a thermal conductivity of 1.5 W/mK, nearly an order of magnitude higher than the surrounding ceramic fiber insulation.

Tables 5 and 6 present a comparison between the sensor data taken from the experiments and the predicted data simulated with the corresponding wattage values.

Temperature differentials across the TEG were determined by finding the magnitude of the difference between sensor 9, the TEG hot plate, and sensor 10, the TEG cold plate. Temperature differentials across the system were determined by the absolute difference between sensor 9 and sensor 1, the deepest sensor.

**Table 5**

Predicted (simulated) vs. actual (experimental) temp. differentials (in ° C).

Location	Exp No. 1 / Sim No. 6		Exp No. 2 / Sim No. 4	
	Predicted	Actual	Predicted	Actual
Across the TEG	14	12	10	13
Across the system	57	59	44	29

**Table 6**

Predicted (simulated) vs. actual (experimental) temperatures (in ° C) for each sensor.

Sensor No.	Exp No. 1 / Sim No. 6		Exp No. 2 / Sim No. 4	
	Predicted	Actual	Predicted	Actual
1	32	24	26	27
2	38	19	31	21
3	48	21	41	24
4	64	30	54	29
5	105	22	86	25
6	160	35	130	31
7	234	108	189	104
8	183	41	155	33
9	89	83	70	56
10	75	71	60	43

## V. CONCLUSION

A major potential source of energy for the Artemis program is the use of thermoelectric technology through TEGs. Despite their current lower efficiencies in comparison to other available sources, TEGs are a growing sector in the field of renewable energies and their use is expected to increase dramatically in the years to come. With respect to the Artemis program and its plans for self-sustaining operations, the design and model proposed in this paper fulfill the dual purpose of generating power as well as utilizing waste heat. With the long lifespans of TEGs, such solid-state devices are expected to run long-term without frequent maintenance.

Variants of such a design can be used to provide a source of power for the Artemis Base Camp. This device will assist NASA in powering the various life support and scientific devices for a lunar colony. In both an experimental and simulated environment, the radiator cylinders were able to

create a useful temperature differential across the TEG modules with a much smaller environmental temperature differential than exists in actual lunar soil.

Increasing the surface area in contact between supporting parts for the TEG cold plate (such as the copper radiator cylinders) and the surrounding soil increases possible points of heat dispersion between the cold plate and the lunar soil; with the effective increase in the cold plate-to-soil contact area facilitated by the copper radiator cylinders' high thermal conductivity and low specific heat, a stronger outgoing heat flux can be established. This is mirrored in reverse by the addition of heat-capturing parts on the TEG hot plate; analogous to the use of a kitchen funnel, increasing the contact area between the heat input and the TEG hot plate allows for a stronger ingoing heat flux.

Utilizing high-thermal conductivity intermediaries such as copper radiator cylinders, systems focused on maintaining low temperatures at acceptable ranges for machinery and other processes will aim to take advantage of increased cold plate-to-soil contact area while systems focused on maximizing raw power output will aim to take advantage of increased heat input-to-hot plate contact area.

Future research could consider more optimized geometries for the radiator cylinders and the HTB, better semiconducting material for the TEG module itself, and other methods of applying waste heat from other processes to the TEG module.

Supplementary materials made throughout the course of this research can be found through this link: [[https://drive.google.com/drive/folders/11laJxTejW7y0n7\\_OHwUXZdO-B0Ej9r1W?usp=sharing](https://drive.google.com/drive/folders/11laJxTejW7y0n7_OHwUXZdO-B0Ej9r1W?usp=sharing)].

#### CRedit AUTHORSHIP STATEMENT

**Eliazar Montemayor:** Conceptualization, Methodology, Validation, Investigation, Resources, Writing - Original Draft, Writing - Review & Editing, Visualization, Supervision, Project Administration, Funding Acquisition. **Matthew Lewton:** Conceptualization, Methodology, Validation, Formal Analysis, Investigation, Resources, Writing - Original Draft, Writing - Review & Editing, Project Administration. **Kane Timlin:** Methodology, Software, Formal Analysis, Investigation, Resources, Data Curation, Writing - Original Draft, Visualization.

#### ACKNOWLEDGEMENT

This work was supported in part by the National Aeronautics and Space Administration through the NASA MINDS program under Cooperative Agreement 80NSSC20M0194 and in part by Montgomery College under authorization by the Dean of Science, Engineering, and Technology. The authors would like to thank Gary Thai for mentorship of this project and the authors' original team that contributed during the NASA MINDS program: Teresa Doley, Marco Lapcevic, Bryan Sanchez, Ryan Phillip, and Alex

Gutierrez. The authors would also like to thank: Dr. David Kuijt, Dr. Led Klosky, Dr. Mustafa Al-Adhami, Sophia Meytin, Burcu Crothers, and Dr. Arturo Rankin for their help.

#### REFERENCES

- [1] National Aeronautics and Space Administration. (2020). Artemis III: Science definition team report. National Aeronautics and Space Administration. Retrieved from <https://www.nasa.gov/sites/default/files/atoms/files/artemis-iii-science-definition-report-12042020c.pdf>
- [2] Vaniman, D., Reedy, R., Heiken, G., Olhoeft, G., & Mendell, W. (1991). Lunar Sourcebook: A user's guide to the moon. Cambridge University Press. Houston, TX: Lunar and Planetary Institute.
- [3] National Aeronautics and Space Administration. (2020). NASA's plan for sustained lunar exploration and development. National Aeronautics and Space Administration. Retrieved from [https://www.nasa.gov/sites/default/files/atoms/files/a\\_sustained\\_lunar\\_presence\\_nspc\\_report4220final.pdf](https://www.nasa.gov/sites/default/files/atoms/files/a_sustained_lunar_presence_nspc_report4220final.pdf)
- [4] Zhang, W. (2019). Lunar subsurface temperature profile modelling based on CE-1 and CE-2. *Bollettino Di Geofisica Teorica Ed Applicata*, 60(3), 489–516. <https://doi.org/10.4430/bgta027>.
- [5] Klosky, J. L. (1997). Behavior of composite granular materials and vibratory helical anchors [Doctoral thesis]. Boulder, CO: University of Colorado.
- [6] Bossinas, L. (1990). Solar power for lunar living [Illustration]. National Aeronautics and Space Administration. Retrieved from [https://www.nasa.gov/centers/glenn/multimedia/artgallery/lunar\\_solar\\_array.html](https://www.nasa.gov/centers/glenn/multimedia/artgallery/lunar_solar_array.html)
- [7] Lunar Surface Innovation Initiative. (2020, February 20). National Aeronautics and Space Administration. Retrieved from [https://www.nasa.gov/directorates/spacetech/Lunar\\_Surface\\_Innovation\\_Initiative](https://www.nasa.gov/directorates/spacetech/Lunar_Surface_Innovation_Initiative)
- [8] cmwarner. (2020, October 28). Lunar living: NASA's Artemis Base Camp concept. National Aeronautics and Space Administration Blogs. <https://blogs.nasa.gov/artemis/2020/10/28/lunar-living-nasas-artemis-base-camp-concept/>
- [9] Jouhara, H., et al. (2021, February). Thermoelectric generator (TEG) technologies and applications. ScienceDirect. Retrieved from <https://www.sciencedirect.com/science/article/pii/S266620272100001X>
- [10] Serra, P., & González-Cinca, R. (n.d.). Thermoelectric generators for long duration lunar missions. In UPCommons. Retrieved from [https://upcommons.upc.edu/bitstream/handle/2117/181266/Serra19\\_EUC\\_ASS.pdf;jsessionid=EAB0A10646D8E912F4EEB1AF198068B0?sequence=1](https://upcommons.upc.edu/bitstream/handle/2117/181266/Serra19_EUC_ASS.pdf;jsessionid=EAB0A10646D8E912F4EEB1AF198068B0?sequence=1)
- [11] Kumar et al. (2019, April). The design of a thermoelectric generator and its medical applications. ResearchGate. Retrieved March 26, 2021, from [https://www.researchgate.net/publication/332730830\\_The\\_Design\\_of\\_a\\_Thermoelectric\\_Generator\\_and\\_Its\\_Medical\\_Applications](https://www.researchgate.net/publication/332730830_The_Design_of_a_Thermoelectric_Generator_and_Its_Medical_Applications)
- [12] Nuclear power plant. (n.d.). Energy Education. Retrieved from [https://energyeducation.ca/encyclopedia/Nuclear\\_power\\_plant](https://energyeducation.ca/encyclopedia/Nuclear_power_plant)
- [13] Nuclear power is the most reliable energy source and it's not even close. (2021, March 24). Office of Nuclear Energy. Retrieved from <https://www.energy.gov/ne/articles/nuclear-power-most-reliable-energy-source-and-its-not-even-close>
- [14] Most efficient solar panels: solar panel cell efficiency explained. EnergySage. Retrieved from <https://news.energysage.com/what-are-the-most-efficient-solar-panels-on-the-market/#:~:text=Most%20solar%20panels%20are%20between,are%20not%20above%2020%25%20efficiency.>
- [15] Power and thermal systems. Radioisotope power systems. Retrieved from <https://tps.nasa.gov/power-and-thermal-systems/power-systems/>
- [16] Thermoelectric power generator. Britannica. Retrieved from <https://www.britannica.com/technology/thermoelectric-power-generator/Principles-of-operation#ref48990>
- [17] Jaziri, N., et al. (2019). A comprehensive review of thermoelectric generators: technologies and common applications. Retrieved from <https://www.sciencedirect.com/science/article/pii/S2352484719306997#89>